Journal of Magnetism and Magnetic Materials 473 (2019) 119–124

Contents lists available at ScienceDirect

Journal of Magnetism and Magnetic Materials

journal homepage: www.elsevier.com/locate/jmmm

Research articles

Weak ferromagnetism in band-gap engineered α-$(Fe_2O_3)_{1-x}(Cr_2O_3)_x$ nanoparticles

R. Rajesh kumar[a,*], Rishav Raj[b], A. Venimadhav[a,c]

[a] School of Nanoscience and Technology, IIT Kharagpur, Kharagpur, India
[b] Department of Metallurgical and Materials Engineering, IIT Kharagpur, Kharagpur, India
[c] Cryogenic Engineering Centre, IIT Kharagpur, Khargapur, India

ARTICLE INFO

Keywords:
Nanoparticles
Band gap engineering
Pectin
Weak ferromagnetism
Optical properties
Spintronics
Sol-gel

ABSTRACT

We report on the tunable band engineering in α-$(Fe_2O_3)_{1-x}(Cr_2O_3)_x$ nanoparticles. Nanoparticles were prepared by the sol-gel method and stabilised in the hexagonal crystal structure with R-3C space group. At room temperature band-gap studies have shown the narrowing of the band gap from 2.1 eV to 1.6 eV with Cr addition. Compared to antiferromagnetic α-Fe_2O_3 nanoparticles, doping of Cr_2O_3 increases the magnetic hysteresis significantly. Impedance spectroscopic studies have revealed Maxwell-Wagner dielectric relaxation near room temperature. Our results improve the understanding of the structural, optical, dielectric and magnetic properties of Cr-doped α-Fe_2O_3 nanoparticles and illustrates that these nanoparticles have potential candidate in spintronic, optoelectronic, solar cell and photocatalysis applications.

1. Introduction

Metal oxide nanoparticles have huge potential in technological applications because of the interplay between various factors such as shape, size, morphology and crystal structure [1–6]. Among the transition metal oxides, α-Fe_2O_3 (hematite) is abundant in nature, non-toxic, highly resistant to corrosion and stable at room temperature. Fe_2O_3 exists in different polymorphic forms, among them the most important and thermodynamically stable form is iron (III) oxide. It is an n-type semiconductor with a narrow band-gap of 2.1 eV [7,8], with Neel temperature of 950 K. It finds application in wide varieties of uses like gas sensors [9], water splitting [10], anode material for lithium-ion batteries [11], photocatalyst [12], electron transport layer in solar cell [13], super capacitor [14] and superparamagnetic nanoparticle for drug delivery application [15,16]. Chromium oxide (Cr_2O_3) is a p-type semiconductor with a wide band gap of 3.4 eV and has many applications including as a gas sensor [17], for protective coating [18], cathode for lithium cells [19] and as a catalyst for industrial processes [20].

The solid solution of the metal oxide is gaining interest to combine its different functional properties in one material to achieve novel electronic states that otherwise do not exist in the parent compounds [21]. In recent years, solid solution of $(Fe_2O_3)_{1-x}(Cr_2O_3)_x$ which is totally mixable in the entire phase diagram due to its similar ionic radius and has become an intense field of research because of the narrowing of the band-gap [22,23], photoconductivity properties [22,23], photocurrent and type-II band alignment [23,24]. To the best of our knowledge, complete studies on the correlation between the band -gap and magnetic property in the nanoparticles have not been conducted so far.

In this paper, we have studied the structural, dielectric, band gap and magnetic properties of the Cr- doped Fe_2O_3 (i.e., $(Fe_2O_3)_{1-x}(Cr_2O_3)_x$) nanoparticles to get a clear understanding of the origin of ferromagnetic ordering for the spintronic applications.

2. Experimental and characterisation

2.1. Experimental synthesis

$(Fe_2O_3)_{1-x}(Cr_2O_3)_x$ ($0 \le x \le 1$) samples (named Cr0, Cr01, Cr02, Cr05 and Cr10 for Cr-concentration X = 0, 0.1, 0.2, 0.5 and 1, respectively) have been synthesised by sol-gel method. An appropriate proportion of analytical-grade metal nitrates $Cr(NO_3)_2{\cdot}6H_2O$ (purity ~99.9%) and $Fe(NO_3)_2{\cdot}6H_2O$ (purity ~99.9%) was mixed thoroughly. The precursors were mixed with pectin and pH is adjusted to 7 and heated overnight to obtain the gel. The obtained gel was washed several times with ethanol and distilled water to remove unreacted precursors and dried in an oven. The oven dried materials were then heated to 400 °C for 2 h to obtain the nanoparticles.

* Corresponding author.
E-mail address: r.g.rajeshkumarr@gmail.com (R.R. kumar).

https://doi.org/10.1016/j.jmmm.2018.10.007
Received 6 September 2018; Received in revised form 1 October 2018; Accepted 1 October 2018
Available online 03 October 2018
0304-8853/

2.2. Characterisation

Phase purity and grain size were studied by X-ray diffraction (XRD) technique, where a Philips PANalytical diffractometer equipped with Cu Kα radiation was used as the X-ray source (Cu = 1.5405 Å). Magnetic measurements were carried out on a commercial VSM SQUID magnetometer (Quantum Design, USA). Transmission electron microscopic studies were carried out using HRTEM, JEOL, Musashino 3-chrome, Akishima, Tokyo, Japan. UV–Vis-NIR spectrophotometer studies were performed on a Varian Cary 5000, in diffuse reflectance spectra (DRS) mode in a range from 200 nm to 2000 nm using the Praying Mantis diffuse reflectance attachment. Dielectric measurements were carried out in the temperature range of 77 K–390 K using an Agilent HP4294A impedance analyser from 40 Hz to1 MHz. High purity silver paste contacts were applied to both faces of the pellet to form parallel capacitance geometry.

3. Results and discussion

3.1. X-ray diffraction

The crystal structure and purity of the prepared nanoparticle were analysed using X-ray diffraction (XRD). The room temperature XRD patterns of $(Fe_2O_3)_{1-x}(Cr_2O_3)_x$ ($0 \le x \le 1$) nanoparticles are shown in Fig. 1. The patterns were recorded in the range of 2Θ from 20° to 80° and all the peak positions of Cr-doped Fe_2O_3 correspond to the standard Bragg positions of corundum Fe_2O_3 with R-3C space group with standard JCPDS (card no #33-0664). From Fig. 1 and Rietveld refinement shows that addition of Cr keeps the hexagonal corundum structure as that of parent Fe_2O_3. The crystallite size of the nanoparticle extracted from XRD shows the size to be of 34 nm for Cr20 and 15 nm for Cr10 respectively [25]. Fig. 2(b) reveals a small decrease in both 'a' and 'c' lattice parameters, correspondingly the volume also decreases [26].

This can be expected due to smaller size of Cr (0.615 Å) compared to Fe (0.645 Å). In Fe_2O_3, all the Fe ions are in octahedral position with increase in Cr concentration, and Cr replaces the octahedral position of Fe and the decrease in size of the octahedral directly corresponds to the decrease in bond angles. The linear variation in lattice constant 'a' and 'c' with increasing Cr-concentration confirms the Vegard's law.

3.2. Transmission electron microscopy

The morphology and the microstructure of the nanoparticles have been examined by transmission electron microscopy (TEM). Characteristic TEM, HRTEM and SAED images of Cr10 and Cr02 nanoparticles are presented in Fig. 3(a)–(d).

The Fig. 3(a) and (d) represents the TEM images of Cr1 and Cr02 nanoparticles. The images show that the nanoparticles tend to coalesce into aggregates and it is common in magnetic nanoparticles.

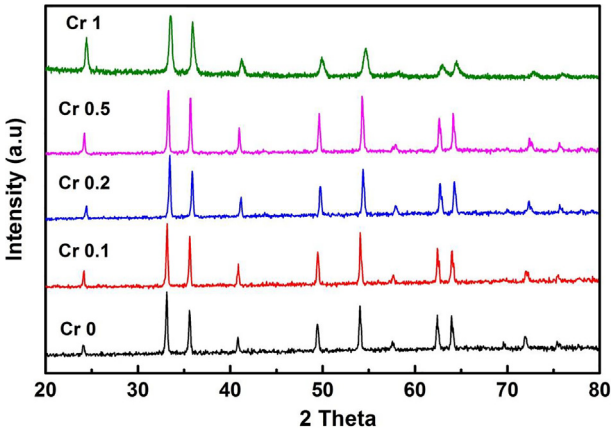

Fig. 1. Room temperature XRD pattern of the nanoparticles with increasing the Cr concentration.

Fig. 3(a) nanoparticle shows that the, synthesised Cr10 sample have well defined spherical shape with uniform distribution. The average particle distribution was determined by ImageJ software and the Gaussian fit of the average particle distribution is shown in insert of the Fig. 3(a), where the average particle size was 6 nm with a standard deviation of 0.75 ± 105 nm.

Closer observations of TEM images of Cr02 nanoparticles at different spots of the sample show an elliptic and shape smooth surface. These nanoparticles contain very developed grain boundaries and free surfaces. The average particle size is 36 nm and the Gaussian fit shows a standard deviation of 1.38 ± 0.689 nm; these are shown in the insert of Fig. 3(d).

The average crystallite size obtained from the TEM measurements corroborates with the value estimated from the XRD study. The HRTEM micrographs of a single crystallite of Cr10 and Cr02 nanoparticles (Fig. 3(b) and (e), respectively) show that the d-value of 0.1961 nm for (2 0 2) plane and 0.2413 nm for (0 0 6) plane which are in good agreement with the XRD pattern. The SAED (selected area electron diffraction) pattern of both particles is indexed with the corundum crystal planes.

The HRTEM and (SAED) patterns also indicates that all the nanoparticles are single crystalline in nature (see Fig. 3(c) and (f) for Cr10 and Cr02, respectively)

3.3. Magnetic property studies

Zero field cooled (ZFC) and field cooled magnetisation (FC) curves of Cr01, Cr02, Cr05 and Cr10 nanoparticles measured in a field of 100 Oe in the temperature range of 10–400 K are shown in Fig. 4. The ZFC and FC curves show an increase in magnetisation and large bifrubrication at low temperature and do not merge even up to 400 K. The Morin transition is observed in hematite around 250 K is found to be absent in all the chromium doped compositions. The parent sample (CrO) with average particle size of ~100 nm exhibits Morin transition at 250 K is shown in the insert of Fig. 5(a) [27]. The Morin transition is a result of spin-flop of spins from a axis to c axis in Fe_2O_3.

While this transition is absent in Cr_2O_3 where all the spins are in the c direction. Hence addition of chromium in the Fe_2O_3 can lead to frustration and can result in canted spins. The bifurcation up to 400 K suggests that Neel temperatures of the samples are above 400 K [28]. This is expected as the composition with the maximum chromium (Cr10) has a transition temperature > 500 K [29].

We have measured the isothermal field dependent magnetisation M (H) measurements at high magnetic fields upto 7 Tesla for all nanoparticles as shown in Fig. 6. Here, the M(H) loops at 300 K illustrate the hysteresis behaviour has large coercive field (Hc) ~2.5 KOe and non-zero remnant magnetization of 0.0062 μB/f.u for the parent. At high fields, a linear increase of magnetisation with non-saturation tendency is noticed. With doping of Cr the Hc value increases to 4.3 KOe in the case of Cr02. The observed weak ferromagetism (WFM) component is attributed to the departure of spin structure, i.e., canting of the magnetic moments from the collinear AFM ordering. The observed magnetic state with different magnetic phases can be represented as total magnetisation:

$$M = \chi_{AFM} H + \sigma_s \quad (1)$$

where $\chi_{AFM}H$ is the AFM contribution and σ_s ,the saturation magnetisation of the WFM phase [30]. The WFM contribution at different temperatures can be obtained by fitting the initial magnetisation curves to Eq. (1) and subtracting the AFM linear part (extrapolated from high fields) from the experimental raw data of initial curve. Inset to Fig. 6(b) shows the field dependent experimental data of initial curve and the extracted AFM and WFM components.

It has been found from our experiments that saturation